Check for updates

Global Biogeochemical Cycles®

RESEARCH ARTICLE
10.1029/2021GB006972

Improving Predictions of Stream CO_2 Concentrations and Fluxes Using a Stream Network Model: A Case Study in the East River Watershed, CO, USA

Brian Saccardi[1] **and Matthew Winnick**[1]

[1]Department of Geoscience, University of Massachusetts, Amherst, MA, USA

Key Points:

- We present a stream network model that accurately predicts stream pCO_2 and fluxes through representation of physical hydrologic processes
- Relationships between pCO_2 and atmosphere exchange velocities result in overestimates of CO_2 fluxes from statistical upscaling methods
- Model-data comparisons suggest that internal CO_2 sources account for half of watershed CO_2 fluxes through benthic hyporheic respiration

Supporting Information:

Supporting Information may be found in the online version of this article.

Correspondence to:

B. Saccardi,
bsaccardi@umass.edu

Citation:

Saccardi, B., & Winnick, M. (2021). Improving predictions of stream CO_2 concentrations and fluxes using a stream network model: A case study in the East River watershed, CO, USA. *Global Biogeochemical Cycles*, *35*, e2021GB006972. https://doi.org/10.1029/2021GB006972

Received 5 FEB 2021
Accepted 22 NOV 2021

Author Contributions:

Conceptualization: Matthew Winnick
Data curation: Brian Saccardi, Matthew Winnick
Formal analysis: Brian Saccardi, Matthew Winnick
Funding acquisition: Matthew Winnick
Methodology: Matthew Winnick
Project Administration: Matthew Winnick
Supervision: Matthew Winnick
Validation: Brian Saccardi, Matthew Winnick
Visualization: Brian Saccardi, Matthew Winnick
Writing – original draft: Brian Saccardi
Writing – review & editing: Brian Saccardi, Matthew Winnick

© 2021. American Geophysical Union. All Rights Reserved.

Abstract Inland waters are an important component of the global carbon budget. However, our ability to predict carbon fluxes from stream systems remains uncertain, as pCO_2 varies within streams at scales of 1–100 m. This makes direct monitoring of large-scale CO_2 fluxes impractical. We incorporate CO_2 input and output fluxes into a stream network advection-reaction model, representing the first process-based representation of stream CO_2 dynamics at watershed scales. This model includes groundwater (GW) CO_2 inputs, water column (WC), benthic hyporheic zone (BHZ) respiration, downstream advection, and atmospheric exchange. We evaluate this model against existing statistical methods including upscaling and multiple linear regressions through comparisons to high-resolution stream pCO_2 data collected across the East River Watershed in the Colorado Rocky Mountains (USA). The stream network model accurately captures GW, evasion, and respiration-driven pCO_2 variability and significantly outperforms multiple linear regressions for predicting pCO_2. Further, the model provides estimates of CO_2 contributions from internal versus external sources suggesting that streams transition from GW- to BHZ-dominated sources between 3rd and 4th Strahler orders, with GW, BHZ, and WC accounting for 49.3%, 50.6%, and 0.1% of CO_2 fluxes from the watershed, respectively. Lastly, stream network model atmospheric CO_2 fluxes are 4-12x times smaller than upscaling technique predictions, largely due to relationships between stream pCO_2 and gas exchange velocities. Taken together, this stream network model improves our ability to predict stream CO_2 dynamics and efflux. Furthermore, future applications to regional and global scales may result in a significant downward revision of global flux estimates.

Plain Language Summary Rivers and streams are an important part of the global carbon cycle, contributing carbon dioxide to the atmosphere. However, the amount of carbon dioxide these systems contribute is notoriously difficult to measure as it changes over short spatial scales. In this paper we present a method of modeling carbon dioxide that uses the current understanding of sources, transport, and reactions that carbon dioxide undergoes in these systems. This model is compared to previous methods of predicting carbon dioxide contributions from streams, using data collected in the East River Watershed in the Colorado Rocky Mountains. We find that the process-based model presented here is more accurate than current methods of predicting carbon dioxide contributions from rivers to the atmosphere. Furthermore, the model suggests that carbon dioxide produced within the stream corridor, as opposed to soil and groundwater sources, contributed roughly half of watershed stream carbon dioxide fluxes. Finally, we show that previous methods for modeling stream carbon dioxide overestimate watershed fluxes by as much as 12x in the East River; therefore, the application of a process-based model to larger systems may result in decreased global estimates of stream carbon dioxide fluxes.

1. Introduction

Inland waters have been recognized as an important component of the carbon cycle, connecting terrestrial carbon (C) to the oceans and atmosphere (Cole et al., 2007). Among inland waters, rivers and streams are the largest contributors of CO_2 accounting for 70% of total fluxes (Raymond et al., 2013). Within rivers and streams, headwaters are often considered hotspots of CO_2 evasion contributing roughly 30% of the 0.7–3.88 Pg of C yr^{-1} inland waters emit to the atmosphere (Drake et al., 2018; Lauerwald et al., 2015; Marx et al., 2017; Raymond et al., 2013). Currently efforts to monitor and predict CO_2 fluxes depend on accurate stream pCO_2 estimates derived from pH, temperature, and alkalinity (Marx et al., 2017; Raymond et al., 2013) or using direct measurements (Hunt et al., 2017; Johnson et al., 2010; Sawakuchi et al., 2017). As CO_2 is often controlled by processes that change

in space and time such as stream turbulence, metabolism, and groundwater inputs (Bernhardt et al., 2018), these measurements are not feasible to deploy at the scales (10^0–10^2 m) required to capture the spatial variability of pCO_2 within stream networks. Due to this inability to measure stream CO_2 with adequate resolution, global fluxes remain highly uncertain and are continuously revised using new statistical scaling models and river data products (Allen & Pavelsky, 2018; Horgby, Segatto, et al., 2019; Sawakuchi et al., 2017). While the processes that control CO_2 variability and fluxes along stream networks are relatively well characterized, current flux budgets rely exclusively on empirical and statistical upscaling or modeling efforts.

Specifically, efforts to quantify large-scale stream CO_2 fluxes generally employ one of two methodologies: statistical upscaling or multiple linear regression analysis. Upscaling efforts typically use statistical distributions of pCO_2 observations, often categorized by Strahler stream order, and apply these to unmeasured regions (Butman & Raymond, 2011; Raymond et al., 2013). Alternatively, a number of studies have used statistical regressions to predict pCO_2 based on readily available environmental variables such as elevation, soil organic carbon content, discharge (Q), and areal wetland extent (Borges et al., 2015; Horgby, Segatto, et al., 2019; Rocher-Ros et al., 2019). In both cases, fluxes are then calculated based on estimated pCO_2 and calculated gas transfer velocities (k) from stream turbulence and geomorphology (e.g., Raymond et al., 2012; Ulseth et al., 2019). While these methods allow for large-scale flux estimates from relatively coarse resolution observations, recent work has suggested that associated flux estimates involve significant uncertainty (Rocher-Ros et al., 2019). These uncertainties include mismatched scales of pCO_2 and k estimates (Lauerwald et al., 2015; Raymond et al., 2013) and observations that are generally biased towards larger stream systems (Sawakuchi et al., 2017). Additionally, a recent analysis of global pCO_2 observations suggests that inverse relationships between pCO_2 and k values may result in large overestimations of stream CO_2 fluxes using traditional statistical upscaling methods (Rocher-Ros et al., 2019); however, the effects of this relationship on flux estimates have not been directly tested.

While models used to predict fluxes are based primarily on statistical measurements, the processes that control stream CO_2 concentrations and fluxes have been characterized in a number of studies (e.g., Duvert et al., 2018; Horgby, Boix Canadell, et al., 2019; Horgby, Segatto, et al., 2019; Hotchkiss et al., 2015; Raymond et al., 2012). Concentrations of CO_2 in streams are determined by the balance of inputs, including soil and groundwater CO_2 and respiration of organic carbon within the water column and hyporheic zone, and outputs such as atmospheric evasion and photosynthesis. In terms of spatial variability of CO_2 concentrations, evasion rates control where on the landscape pCO_2 is highest or lowest, as pCO_2 may degas over scales of 10's of meters (Johnson et al., 2008; Lupon et al., 2019). A number of studies have found that k values which control evasion, are primarily related to discharge and topography, allowing for large-scale estimates based on hydrographic datasets (Raymond et al., 2012; Ulseth et al., 2019). While evasion exerts a strong control on the spatial variability of CO_2 concentrations and fluxes (Rocher-Ros et al., 2019), integrated fluxes from stream networks, however, are controlled primarily by CO_2 sources.

Sources of stream CO_2 are broadly categorized as either allochthonous or autochthonous, where allochthonous sources are CO_2 dissolved in soil- and groundwater (GW) that is transported to the stream, and autochthonous CO_2 is produced in the water column or within the benthic and hyporheic zones (Marx et al., 2017). While studies have converged on a conceptual model in which autochthonous sources become increasingly important with increasing stream size, the relative balance of these sources remains uncertain (Hotchkiss et al., 2015). For example, in a survey of US hydrologic monitoring sites, Hotchkiss et al. (2015) found that while autochthonous contributions increased with stream size, GW was the dominant source across all sites. Winterdahl et al. (2016) found similar results with groundwater contributing >90% of the CO_2 to boreal headwater systems. In contrast, a recent CO_2 budgeting study of 1st-3rd order streams in the Cote Du Nord region found that autochthonous sources accounted for ~75% of stream CO_2 (Rasilo et al., 2017), and another study found that photoreactions account for 25%–40% of CO_2 fluxes in artic fresh water environments (1st – 3rd order and lakes) (Cory et al., 2014). Lupon et al. (2019) found that headwater streams in a cold humid boreal region had internal and external CO_2 that were more balanced contributing 17%–51% and 34%–66%, respectively. In addition to natural variability between sites, some of this uncertainty is likely due to differences in methods used to partition CO_2 sources (Rocher-Ros et al., 2020), including diel oxygen signals of in-stream metabolism (Hotchkiss et al., 2015), mass balance of calculated (Winterdahl et al., 2016) or measured (Lupon et al., 2019; Rasilo et al., 2017) CO_2, and stream water incubations (Cory et al., 2014). Thus, the lack of constraints on CO_2 source contributions remains a major knowledge gap in terms of our ability to predict stream CO_2 variability.

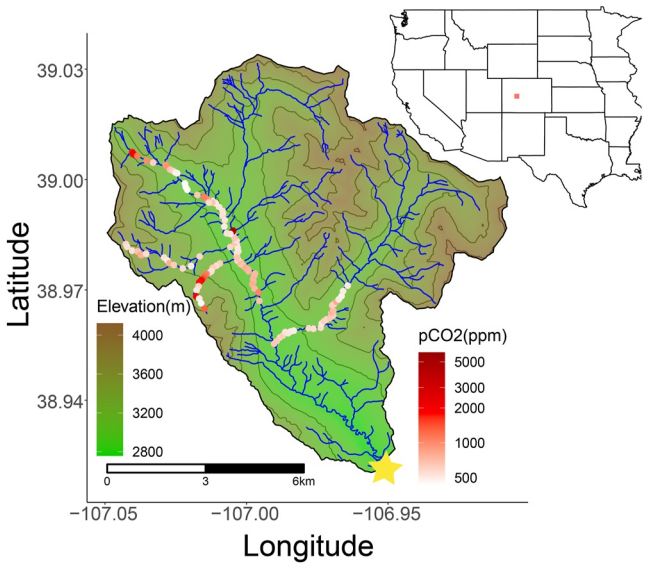


Figure 1. Map of the East River watershed (87 km^2) with NHDplus flow lines of the East River and tributaries shown in blue, shaded elevation contours in green, and field-sampled pCO_2 (ppm) as points colored from white (smallest) to red (largest) (n = 121).

Process-based models that incorporate transport and chemical reactions are extremely useful for disentangling complex natural systems and predicting elemental fluxes (Steefel et al., 2005). The processes controlling CO_2 in river systems, including where and how they operate, are relatively well-defined; therefore, we seek to incorporate these into a predictive model framework. Due to the spatiotemporal variability of pCO_2 and complex set of reactions that govern its fate and transport, we argue that a stream network model is an ideal method of mechanistically modeling pCO_2 in a manner that allows for pCO_2 to be predicted at the high spatial resolution required to accurately calculate landscape fluxes (Rocher-Ros et al., 2019). Beyond predicting pCO_2 and fluxes, stream network models can help to determine the relative importance of CO_2 pathways into streams comparing potential contributions of water column and benthic hyporheic zone (BHZ) respiration along with GW CO_2 inputs. Additionally, stream network models can be used to identify potential hotspots and hot moments to guide fieldwork. In this study, we develop a whole stream network advection-reaction model that predicts stream CO_2 concentrations and effluxes. We apply this model to a mountainous watershed in Gothic, CO (USA) that spans 1st- 5th order streams, and further validate the model against a new high-resolution data set of stream geochemistry. We further compare model results to existing upscaling and multiple linear regression model techniques, and use the model-data comparisons to evaluate the relative importance of internal and external CO_2 sources.

2. Methods

2.1. Field Site Description

This study was conducted in the East River watershed near the Rocky Mountain Biological Laboratory in Gothic, Colorado (USA). The East River watershed delineated at the star shown in Figure 1 is 87 km^2 and includes 1st to 5th Strahler order streams. The watershed ranges in elevation from 2,760 to 4,123 m above sea level, has a mean slope of 23° (Winnick et al., 2017), and is broadly representative of watersheds throughout the Rocky Mountains (Battaglin et al., 2011; Markstrom & Hay, 2009). Snow is the dominant form of precipitation in the basin with an average precipitation of 1.23 ± 0.26 m y^{-1} and an annual average temperature of 1°C (PRISM, 2013). During the sampled period, snow was present in the higher elevations and meltwater was contributing to the discharge (Q). The three major life zones within the basin are alpine, montane, and subalpine (Carroll et al., 2018; Hubbard et al., 2018) with the tree line at 3,500 m (Winnick et al., 2020). The modeled East River watershed comprises a range of land cover including conifer and aspen forests (32%), unvegetated rock (28%), grass and shrubland (23%), and wetlands (16%), with <1% of land as a mixture of human uses (U.S. Geological Survey, 2016) (Figure S1 in Supporting Information S1). The majority of the watershed is underlain by the Mancos Shale formation in which weathering solute fluxes are dominated by calcium carbonate dissolution and pyrite oxidation (Carroll et al., 2018; Morrison et al., 2012; Winnick et al., 2017). Additionally, oxidation of Mancos shale petrogenic organic carbon may contribute to soil and riverine CO_2 fluxes (Hilton et al., 2021). However, the western side of the basin has a greater proportion of Quartz Monzonite Porphyry, and tributaries display lower solute concentration when compared to the rest of the watershed (Carroll et al., 2018; Gaskill et al., 1967, 1991).

2.2. Sampling Methods

Geochemical measurements and stream samples were taken across the East River watershed and its tributaries over a 10-day period in August 2019 during daylight hours (8:00-18:00) (Figure 1). August discharge values range from 1.23 to 3.25 m^{3}s^{-1} at the pumphouse (star in Figure 1) (Carroll et al., 2021) and precipitation during the sampled days totaled 3.3 cm (Newcomer & Rogers, 2020). Samples were taken longitudinally along the stream every ~80 m within the designated reaches. At every site, pH, conductivity, dissolved oxygen (DO), and temperature were taken with a Yellow Springs Instruments multiparameter sensor (YSI Professional Plus) (n = 151). Additionally, direct pCO_2 measurements were taken using an EGM-5 Portable CO_2 Infra-Red Gas

Analyzer (PP Systems). Samples were prepared by equilibrating 80 ml of stream water with 60 ml of atmosphere in a gas-tight syringe, which was shaken vigorously for 60 s before direct injection into the analyzer. Measurements were corrected for atmospheric CO_2 using the method described in Koschorreck et al. (2021) with an atmospheric air pCO_2 of 400 ppm (ambient atmosphere measurements ranged from 400 to 408ppm). For the CO_2 corrections, calculated alkalinity was used if available and the mean alkalinity was used for sites without dissolved inorganic carbon (DIC) measurements. At a subset of points ($n = 54$) DIC and dissolved organic carbon (DOC) samples were collected into amber VOC vials with no headspace using 0.2 µm filters. The DIC/DOC samples were analyzed on an Aurora 1030 (OI Analytical), and DIC was used to calculate alkalinity as described in Plummer and Busenberg (1982).

2.3. Stream Network CO_2 Model

We developed a stream network model based on the advection-reaction equation for solute transport to predict pCO_2 across the East River watershed. These types of models have been recognized as an important method of estimating elemental fluxes by enhancing the spatial and temporal coverage of data (Bencala & Walters, 1983). Changes in $CO_{2(aq)}$ (C; mol/L) through time (t) are calculated as,

$$\frac{dC}{dt} = -v\frac{dC}{dx} + \frac{1}{A}\frac{dQ}{dx}(C_{gw} - C) - k_{CO2}(C - C_{atm}) + F_{wc} + F_{he}, \quad (1)$$

where v is velocity (m s^{-1}), A is stream cross-sectional area (m^2), Q is discharge (m^3 s^{-1}), x is lateral distance (m), C_{gw} and C_{atm} are the molarity of CO_2 in groundwater and atmosphere-equilibrated water, respectively (see Table 1 for model variables and descriptions). The molar fluxes of $CO_{2(aq)}$ (mol L^{-1} s^{-1}) from water column and hyporheic zone net respiration are F_{wc} and F_{he}, respectively (Table 1) with F_{wc} parameterized directly as a set flux of CO_2 and F_{he} parameterized using turbulence-based exchange based on surface renewal theory (Grant, Gomez-Velez, et al., 2018). The reaeration coefficient of CO_2, k_{co2} (s^{-1}), was calculated as the gas transfer velocity of CO_2 divided by stream depth. The gas transfer velocity of CO_2 was estimated using k_{600}, based on the equations of Ulseth et al. (2019):

$$\ln(k_{600})\text{for eD} > 0.02 = 1.18 * \ln(eD) + 6.43, \quad (2)$$

and

$$\ln(k_{600})\text{for eD} < 0.02 = 0.35 * \ln(eD) + 3.10. \quad (3)$$

Here, eD is the energy dissipation rate of the stream (m^2 s^{-3}) calculated as,

$$eD = g * v * s, \quad (4)$$

where g is the acceleration due to gravity (9.8 m s^{-2}), and s is stream slope (unitless, m m^{-1}) calculated at each point from a digital elevation model (DEM) (Horn, 1981). In order to convert k_{600} into k_{CO2}, we calculated the Schmidt number sc_t (unitless) using the average daily air temperature T (13.7°C) of the sampling period and the equation (Wanninkhof, 1992),

$$sc_t = 1911 - 118.11 * T + 3.453 * T^2 - 0.0413 * T^3. \quad (5)$$

The k_{CO2} variable was then calculated using the equation (Raymond et al., 2012),

$$k_{CO2} = \frac{k_{600}}{(600/sc_t)^{-0.5}}, \quad (6)$$

where −0.5 is assumed due to the turbulent surfaces of streams (Jähne et al., 1987; Ulseth et al., 2019).

For hyporheic exchange of CO_2, we assume that fluxes are dominated by turbulent vertical exchange with the benthic hyporheic zone. First, bar and sinuosity-driven exchange likely feature reduced exchange fluxes and typical transit times that are greater than reaction times, limiting their influence on stream CO_2 fluxes (Gomez-Velez & Harvey, 2014; Gomez-Velez et al., 2015). Vertical exchange, in contrast, features a combination of relatively large exchange fluxes along with residence times comparable to reaction times, leading to efficient CO_2 generation (Gomez-Velez et al., 2015; Harvey et al., 2013, 2019). Turbulence driven hyporheic exchange, in particular,

Table 1
Parameters Used in the Model With "Value, Unit" Column Showing the Equation or Value Used in the Model and the "Range" Column Showing the Ranges Outputted From the Model or the Ranges Used in the Optimization

Variable	Description	Value, unit	Range	Data source
A	Stream cross-sectional area	m^2	0.002–2.288	
C_{atm}	Atmospheric $CO_{2(aq)}$	$2.13e^{-5}$, mol L^{-1}	–	
C_{gw}	Groundwater $CO_{2(aq)}$	0.0012, mol L^{-1}	0.0006–0.0009	Optimization
C_{hz}	Hyporheic $CO_{2(aq)}$	$3.7e^{-5}$, mol L^{-1}	$1.1e^{-5}$–$5.3e^{-5}$	Optimization
$C_{wetland}$	Wetland groundwater $CO_{2(aq)}$	0.0025, mol L^{-1}	0.0021–0.0027	Optimization
DA	Change in area over change in length	m	$3.23e^{-7}$ –$1.05e^{-4}$	DEM
D_m	Molecular diffusion coefficient of CO_2 in water	$1.6e^{-9}$, m^2 s^{-1}	–	Grant, Gomez-Velez, et al. (2018)
eD	Energy dispersion rate of the stream	Equation 4, m^2 s^{-3}	0–4.95	Horgby, Segatto, et al. (2019)
F	Watershed CO_2 fluxes	Equation 15, Moles C	–	
F_{he}	Hyporheic zone molar fluxes of $CO_{2(aq)}$	Equation 8, mol L^{-1} s^{-1}	0–0.016	
F_{wc}	Water column molar fluxes of $CO_{2(aq)}$	$9e^{-11}$, mol L^{-1} s^{-1}	$3.4e^{-11}$– $3.4e^{-9}$	Optimization, Reisinger et al. (2015), Ward et al. (2013)
g	Gravitational acceleration	9.8, m s^{-2}	–	
h	Stream depth	Equation 13, m	0.03–0.35	Horgby, Segatto, et al. (2019)
K_{600}	Gas transfer velocity corrected to 20°C	Equation 2/3, m d^{-1}	0–0.20	Horgby, Segatto, et al. (2019)
K_{CO2}	Gas transfer velocity of CO_2	Equation 6, m d^{-1}	0–0.17	Ulseth et al. (2019)
k_{hz}	Hyporheic zone gas transfer velocity	Equation 9, m d^{-1}	0–0.003	Grant, Gomez-Velez, et al. (2018)
Q	Discharge	m^3 s^{-1}	0.01–1.95	
s	Stream slope	[a]	0–1.81	DEM
sc_t or sc	Schmidt number	Equation 5/10, [a]	834.8 or 812	Grant, Gomez-Velez, et al. (2018)
T	Temperature	13.7, °C	–	
u	Shear velocity	Equation 11, m s^{-1}	0–1.5	Grant, Azizian, et al. (2018)
v	Stream velocity	Equation 12, m s^{-1}	0.01–0.85	Horgby, Segatto, et al. (2019)
w	Stream width	Equation 14, m	0.06–6.62	
x	Distance	m	–	

[a]unitless.

is generally restricted to the shallowest portion of benthic sediments, though depths of mixing are controlled by a number of factors (Breugem et al., 2006). While short transit times, likely on the order of seconds to an hour, may limit the extent of chemical reactions (Harvey et al., 2019), fast aerobic respiration rates compounded by higher respiration rates within the shallowest benthic depths may act to increase their role in overall fluxes (Li et al., 2017). Turbulence-based models have shown promise in explaining benthic DO profiles (O'Connor & Hondzo, 2008), limits to hyporheic zone denitrification (Grant, Azizian, et al., 2018), conservative tracer tailing patterns (Roche et al., 2019), and N_2O yields from hyporheic zone denitrification (Winnick, 2021). Further, models of turbulent exchange have the potential to be highly scalable (e.g., Grant, Gomez-Velez, et al., 2018; Packman et al., 2004) and involve relatively low data requirements (Grant, Azizian, et al., 2018). We therefore employ a parameterization of turbulent exchange based on surface renewal theory from Grant, Gomez-Velez, et al. (2018):

$$F_{he} = k_{hz}(C_{hz} - C), \tag{7}$$

where C_{hz} is the molarity of CO_2 in the benthic hyporheic zone and k_{hz} is the benthic hyporheic zone mass transfer coefficient (m s^{-1}). Within this parameterization, k_{hz} is calculated as,

$$k_{hz} = 0.17u * Sc^{-2/3}, \tag{8}$$

where u is the shear velocity (m s^{-1}). The Sc term is calculated as,

$$Sc = \frac{kv}{D_m}, \tag{9}$$

where kv is kinematic viscosity of water ($m^2\ s^{-1}$) and D_m is molecular diffusion coefficient of CO_2 in water ($m^2\ s^{-1}$). Shear velocity is calculated as,

$$u = \sqrt{ghs}, \tag{10}$$

where s is slope (unitless, $m\ m^{-1}$), and h is depth (m).

Equation 1 was solved assuming steady state conditions using a backwards-difference finite approximation scheme,

$$0 = -v\left(\frac{C_i - C_{i-1}}{\Delta X}\right) + \frac{1}{A}\left(\frac{\Delta Q}{\Delta X}\right)(C_{gw} - C_i) - k_{CO2}(C_i - C_{atm}) + F_{wc} + k_{hz} * (C_{hz} - C_i), \tag{11}$$

with i and i-1 representing a grid cell and the previous grid cell respectively.

In sum, the final model used for this research includes advection, evasion, GW inputs, water column respiration, and turbulent hyporheic exchange with the benthic hyporheic zone. Carbonate equilibrium was not included in the model as it was assumed that additional CO_2 inputs from speciation effects would be small (Stets et al., 2017) compared to the GW and BHZ inputs as the effects of speciation are minimal when alkalinity is below 2,000 μeq/L. These assumptions are supported in the East River watershed as calculated alkalinity from measured DIC was below 2,000 μeq/L at all but one site. However, carbonate equilibrium would likely need to be considered in streams with alkalinity significantly above 2,000 μeq/L.

In order to predict pCO_2 across the watershed, we solved Equation 11 for every grid cell sequentially along each reach starting with 1st order streams. The initial C_i in the first grid cell within 1st order streams was set to C_{gw}, and C_i values at stream junctions were calculated as the discharge-weighted mean of all contributing stream model cells. The grid cells were set using flow line vertices from the NHDplus data set (U.S. Geological Survey, 2019) which resulted in variable grid spacing with 392 stream reaches and 7,969 model grid cells. Topographic information for each grid cell such as slope and elevation were retrieved and calculated from a 10m DEM.

Due to ongoing snowmelt in the upper basin that lagged snowmelt at lower elevations during our sampling campaign in August 2019, we used elevation to estimate local contributing runoff (m/s) using a linear regression as snow in the high elevations led to increased Q (Figure S2 in Supporting Information S1). This resulted in runoff estimates ranging from 0.1 to 0.4 cm/day across the watershed (Carroll & Williams, 2019). The change in discharge along stream reach ($\Delta Q/\Delta x$ in Equation 7) was calculated as local runoff multiplied by the NHDplus reach upstream accumulating area per unit length of the stream reach. Discharge at each grid cell was calculated as the discharge at the previous grid cell plus runoff-based groundwater inputs, assuming constant gaining conditions. The modeled Q was compared to discharge data at 6 locations in the watershed measured in August 2019 and was strongly correlated ($R^2 = 0.99$) (Figure S3 in Supporting Information S1; Carroll et al., 2021).

The stream width (w), depth (h), and velocity (v) in meters were calculated using scaling relationships from Horgby, Segatto, et al. (2019) for mountainous streams as,

$$v = 0.668 * Q^{0.365}, \tag{12}$$

$$h = 0.298 * Q^{0.222}, \tag{13}$$

and

$$w = Q/v/h. \tag{14}$$

The calculated v along with k_{CO2} was additionally used to determine stream CO_2 half-life distance at each point using a first order reaction,

$$\text{half life} = \frac{ln(2)}{k_{CO2}/v} \tag{15}$$

representing the distance over which stream CO_2 evades to half its concentrations assuming no additional CO_2 inputs (Figure S4 in Supporting Information S1).

The model was further amended to capture observed field conditions including wetland and snow plug locations. Specifically, wetlands are often sources of elevated CO_2 in groundwater (Buffam et al., 2010; Hope et al., 2004), and snow plugs may act to trap CO_2 in the stream environment by limiting water-atmosphere interfaces. Snow plugs were defined as large areas of snow covering the stream, and modeled k_{CO2} was set to 0 where snow plugs were noted. This k_{CO2} correction was conducted to better represent field conditions and did not affect integrated CO_2 fluxes. Stream sections that were within perennially saturated organic-rich fens were modeled using $C_{wetland}$ in place of C_{gw}. Lastly, NHDplus headwater flowlines were trimmed to match points of stream emergence recorded in the field.

Within all the above model equations there are four free parameters: CO_2 concentrations in GW, wetlands, and the benthic hyporheic zone relative to the stream, along with water column respiration fluxes. To tune the model, we simulated 600 model runs across variable ranges of 5,000–50,000 ppm, 10,000–100,000 ppm, $9*10^{-11}$–$3.4*10^{-9}$ mol L^{-1} s^{-1}, and 0–2,000 ppm for C_{GW}, C_{wet}, F_{wc}, and (C_{hz} – C), respectively. The simulation summary table is included in Data Set S2. We chose the optimized values based on maximum coefficients of determination (R^2) and minimum Root Mean Square Error (RMSE) from model-data comparisons described below. Additionally, the model was run using the maximum WC respiration to determine its potential importance. Model R code version 3.6.3 (2020-02-29) along with NHDplus hydrography datasets for the basin are included in Supporting Information S1. Optimized values were further compared and validated against field observations and data from previous publications as described in the Results section.

2.4. Statistical Analyses

In order to compare the model output to our sampled points, GPS locations of the sampled points were paired with their closest model grid cell. The paired points were filtered to remove any that were more than 50 m apart, or for which there was no NHDplus counterpart (n = 30). Points without NHDplus counterparts comprised seeps and small streams that were not represented by NHDplus flowlines. The remaining 121 points of which 12, 23, 21, and 65 are 1st – 4th order respectively, were compared using model-data R^2, RMSE, and t-tests to the stream network model with and without BHZ respiration and water column respiration to determine if the addition of internal processes add predictive power to the model. All calculations were conducted using R (R Core Team, 2020; Supporting Information S1).

A multiple linear regression model (MLRM) predicting pCO_2 based on Q, velocity, slope, elevation, and mean watershed net primary production (NPP) (NASA, 2019) was determined using a stepwise approach. Using Q, k_{CO2}, velocity, slope, elevation, stream order, k_{hz}, mean watershed NPP, and landcover as the initial inputs, all possible regression combinations were calculated. The best regression model was chosen based on the lowest AIC value that contained only significant predictors ($p < 0.05$). The final regression was evaluated by calculating the mean and variance of the pCO_2 predicted as well as comparing the R^2 and RMSE values. Additionally, global scale mountainous inland water CO_2 fluxes were recently estimated using an MLRM based on pCO_2 data in the European Alps (Horgby, Segatto, et al., 2019). The regression consisted of elevation, Q, and soil organic carbon (SOC) from Hengl et al. (2017). For comparison, we applied this model to the East River watershed to test the potential scalability of the Horgby MLRM to different field areas. Specifically, this analysis was conducted in order to determine if MLRM's are able to accurately predict CO_2 outside their training data set regions and thus assess potential scalability of regional statistical models.

Additionally, we compared existing statistical upscaling methods for estimating watershed-scale CO_2 fluxes based on point measurements to integrated model outputs. Two common methods of upscaling CO_2 evasion fluxes were evaluated against the stream-network modeled fluxes. The flux estimation methods evaluated used Equation 16 and the same k_{CO2}, h, w, and Δx as the stream network model. In the upscaling models, pCO_2 was calculated as (a) mean pCO_2 from all samples across the watershed; and (b) mean stream pCO_2 by Strahler order (Butman & Raymond, 2011; Raymond et al., 2013). The corresponding CO_2 fluxes were compared to stream network model fluxes for each stream order. The watershed-scale CO_2 evasion fluxes (F) were calculated for the modeled and regression data using the equation,

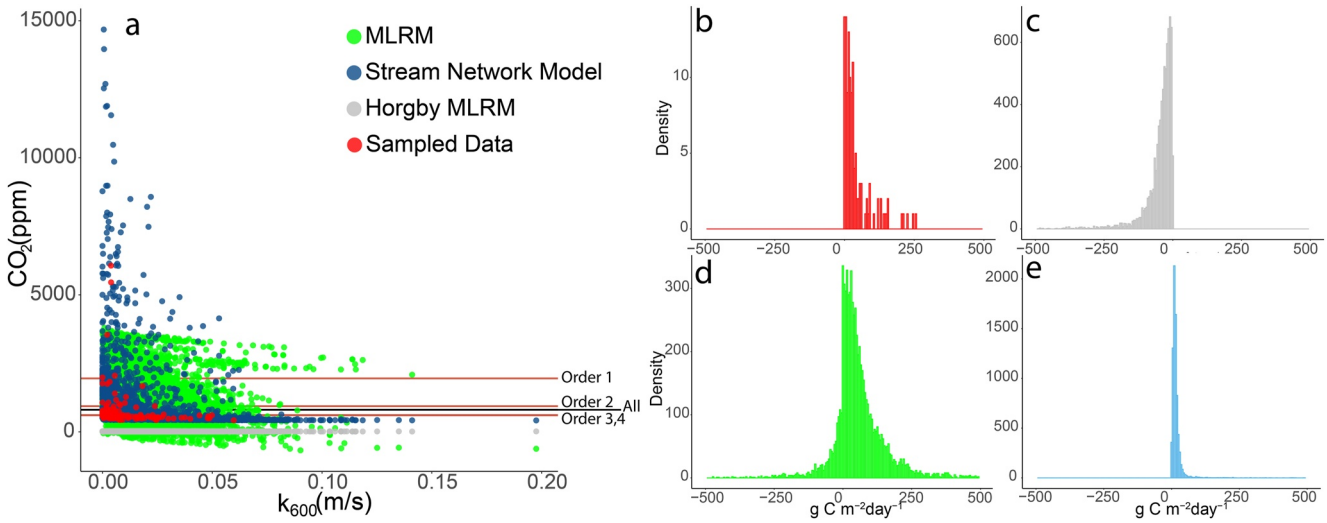


Figure 2. (a) Stream pCO_2 plotted against k_{600} with MLRM in green, stream network model in blue, Horgby MLRM in gray, and sampled data in red. Lines show values used in the upscaling calculations with brown lines representing mean pCO_2 in 1st – 4th order streams top to bottom and the black line is the mean of all sampled pCO_2. Histogram of modeled fluxes are shown on right with (b) sampled data (c) Horgby MLRM in gray (d) MLRM and (e) Stream Network Model.

$$F = \sum (C_i - C_{\text{atm}}) * k_{\text{CO2}} * h * w * \Delta x. \quad (16)$$

Additionally, we repeated the upscaling methods with flux estimates restricted to the reaches with sampled data to evaluate model and upscaling performance within well-characterized areas.

3. Results

3.1. Observational Data

Stream waters across the East River and its tributaries had a mean temperature of 8.1°C ranging from 2.7 to 14°C at elevations ranging from 2,873 to 3,521 m. Across all sample points, the mean dissolved oxygen saturation % (DO) was 91% and ranged from 0.4 to 11.4 mg L^{-1}. The mean pH was 8.03 ranging from 7.14 to 8.4. Roughly 90% of samples were below 8.3, such that bicarbonate was the dominant inorganic carbon species present. Conductivity within the data ranged from 11.6 to 263.1 µs cm^{-1} with a mean of 112.4 µs cm^{-1}. Alkalinity ranged from 270 to 3,013 µeq/L with a mean of 1,064 µeq/L, and all but one site was below 2,000 µeq/L. DIC and DOC ranged from 2.4 to 36.1 mg/L and 0.1–2.8 mg/L with means of 13.3 mg/L and 1.0 mg/L respectively.

Measured pCO_2 was consistently elevated above atmospheric concentrations with a mean of 806 ppm and range of 423–6,066 ppm (Figure 1). First order streams had the highest mean pCO_2 at 1,951 ppm. Increasing stream order generally corresponded to decreasing mean pCO_2, with 2nd-4th order streams having mean pCO_2's of 937, 603, and 613 ppm respectively. The minimum pCO_2 within each order showed little variation, ranging from 429 to 513 with no correlation to stream order; however, the maximum values decreased with increasing stream order with a pCO_2 of 6,066, 2,050, 1,070, and 1,019 ppm in 1st – 4th order streams respectively. Additionally, k_{CO2} was found to correspond to low in-stream pCO_2 as 95% of sampled points with k_{CO2} values of greater than ~0.005 (m/s) had $pCO_2 < 1{,}000$, similar to findings in a Swedish catchment system (Figure 2) (Rocher-Ros et al., 2019).

Point sample data was used to estimate total watershed CO_2 fluxes based on two separate upscaling methods as described above (Butman & Raymond, 2011; Raymond et al., 2013). The first method (Raymond et al., 2013) used the mean sampled pCO_2 and applied it across the entire stream model using the modeled stream morphology and k_{CO2}, which resulted in total watershed fluxes of 16.9 ± 31.8 Mg C day^{-1}. The second method was to predict CO_2 fluxes separately for each stream order using the mean pCO_2 within each order as the orders CO_2 concentration while maintaining the other modeled parameters. This predicted pCO_2 fluxes of 16.7 ± 16.0 Mg C day^{-1} with 1st-5th orders contributing 7.4 ± 9.6, 2.4 ± 2.2, 1.1 ± 1.0, 1.9 ± 1.1, and 3.7 ± 2.1 Mg C day^{-1}, respectively. Additionally, flux predictions were restricted to the 2,508 m of sampled reaches out of the total 164,872 m in the

Table 2
Model Performance With RMSE and R^2 for the Full Data Range and R^2 by Stream Order

	pCO_2 range (ppm)	R^2	P	RMSE	R^2 1st order	R^2 2nd order	R^2 3rd order	R^2 4th order	Fluxes Mg C/day	Sampled reach fluxes Mg C/day
Sampled data	423–6,066	–	–	–	–	–	–	–	–	0.16
Stream network Model	417–18,000	0.7	$<10^{-15}$	763	0.71	0.56	0.51	0.34	3.9	0.08
MLRM	−674–3,795	0.21	$<10^{-7}$	519	0.75	0.03	0.01	0.08	47.9	0.02
Horgby MLRM	12–32	0.27	$<10^{-10}$	1097	0.79	0.03	0	0.02	−16.1	−0.38
Upscaling by mean pCO_2	806	–	–	–	–	–	–	–	16.9	0.39
Upscaling by mean order pCO_2	603–1,951	–	–	–	–	–	–	–	16.7	0.24

Note. Predicted range of pCO_2 and CO_2 flux are shown for each model for the entire watershed and only within the sampled reaches.

modeled East River watershed. These fluxes were calculated by only applying sampled pCO_2 values to their local reaches (mean 21 m) in Equation 16. This was done in order to compare upscaling methods to sampled data on a one-to-one basis (Table 2). This resulted in a prediction of 0.16 Mg C day^{-1} released from the sampled reaches based on measured data. Comparatively, the stream network model predicted emissions of 0.5x as much CO_2 to the atmosphere. Part of this underestimation reflects the fact that field measurements were inherently biased towards flatter stream sections, as a number of steep reaches were inaccessible for sampling. As for the upscaling methods using the mean pCO_2 resulted in a 2.4x increase in estimated CO_2 fluxes relative to observations, and the upscaling which used individual order mean pCO_2 had a 1.5x increase in estimated CO_2 fluxes.

3.2. Model Results

The optimization of the model resulted in a C_{GW} pCO_2 of 18,000 ppm, C_{wet} pCO_2 of 44,000 ppm, F_{wc} of $9*10^{-11}$ mol L^{-1} s^{-1}, and a benthic hyporheic zone pCO_2 elevation ($C_{hz} - C$) of 700 ppm. The best three optimization runs all had the same C_{GW} and C_{wet} values, with C_{GW} values falling within the range of sub-soil (>30 cm) growing season pCO_2 values measured in a soil profile within the East River watershed (~7,000–23,000 ppm; Winnick et al., 2020). Point measurements of standing waters within wetland areas were above the 25,000 ppm calibration of the EGM-5, though typically displayed values between 30,000–100,000 ppm supporting the elevated model optimization value. Additionally, wetlands in northern latitudes such as Denmark have recorded pCO_2 ranging from ~20,000 to 180,000 ppm (Elberling et al., 2011) encompassing the optimization value used. As the optimized water column respiration rate was found to be at the lower end of the literature values (Table 1), we ran the stream network model using a rate of $3.4*10^{-9}$ mol L^{-1} s^{-1} which represents the upper limit of the values found in Ward et al. (2013) and Reisinger et al. (2015) as an estimate of the maximum potential water column contributions (Figure S5 in Supporting Information S1). Additionally, The benthic hyporheic zone pCO_2 was found to be elevated above stream pCO_2 by 700 ppm which was comparable to mean hyporheic zone estimates of 695 ppm from 20 cm pore waters in the East River based on data from Nelson et al. (2019) using pCO_2 values calculated from measured pH and estimated alkalinity (see Figure S6 in Supporting Information S1).

The full model including benthic hyporheic and water column respiration (Figure 3) predicted pCO_2 values and captured observed spatial patterns with a lower RMSE and higher R^2 for $\ln(pCO_2)$ then the GW-only stream network model. Additionally, the full model had a paired t-value of 0.10 (df = 120, $p = 0.93$) while the GW-only model had a paired t-value of 0.18 (df = 120, $p = 0.86$) for pCO_2. The paired t-tests suggest a mean underestimation of 17 ppm between matched points for the GW-only model and overestimation of 6 ppm for the full model with neither model showing significant difference ($p > 0.05$) from the observed pCO_2 values. We note that the model also features a −18 ppm bias at pCO_2 values less than 1,000 ppm, comparable to measurement error (Figure S7 in Supporting Information S1). As the Full model outperformed the GW-only model in all three metrics of validity, from this point on we discuss and analyze the full model.

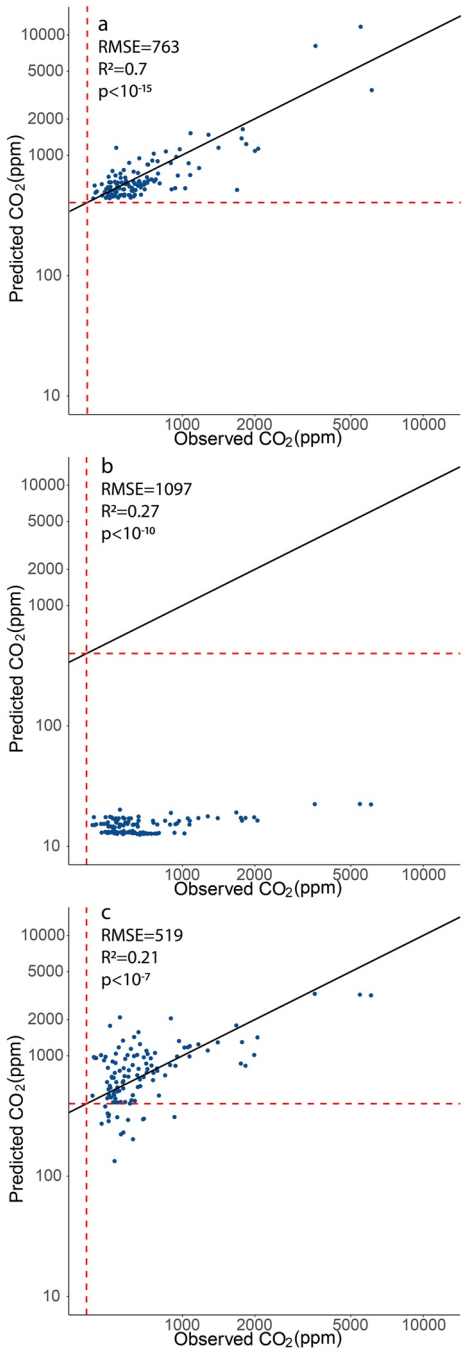


Figure 3. Model-data comparisons and statistics for the (a) stream network model; (b) Horgby MLRM; and (c) MLRM with 3 points missing as they were negative. The dashed lines (red) represent atmospheric pCO_2 (400 ppm) and the solid line (black) is the 1:1 line. RMSE and R^2 are for $\ln(pCO_2)$.

Stream network model pCO_2 was consistently elevated above atmospheric concentrations ranging from 417 ppm to optimized GW values with a mean of 1,097 ppm, compared to the measured range of 423–6,066 ppm (Figure 4). The largest discrepancy between the model and the sampled data were at highest observed pCO_2 locations; however, 95% of modeled points were within 450 ppm above and 950 ppm below the sampled points (Figure S7 in Supporting Information S1). The highest pCO_2 values were predicted in the headwaters at points of spring emergence and quickly approached atmospheric values. Across all model points, the median calculated CO_2 half-life was 11 m. As a result, model pCO_2 was strongly restricted by k_{CO2}; 95% of modeled points with k_{CO2} greater than ~0.005 (s^{-1}) had $pCO_2 < 1{,}000$ ppm (Figure 2).

Modeled patterns were similar to observational data with mean pCO_2 decreasing as stream order increased: 1st-5th order streams had a mean pCO_2 of 1,842, 715, 589, 536, and 478, respectively. Similarly, the max pCO_2 showed a decreasing pattern with stream order with 1st -5th orders having 18,000, 8,781, 2,793, 898, and 554 ppm, respectively. The minimum pCO_2 showed no pattern across orders with 1st -5th order streams having 432, 417, 424, 422, and 422 ppm respectively.

The full stream network model predicted a mean flux of 18.2 g C m^{-2} day^{-1} ranging from 0 to 1,227.5 g C m^{-2} day^{-1} with total watershed fluxes at 3.9 Mg C day^{-1} (Figure 4, Table 2, Text S5 in Supporting Information S1). The highest fluxes were predicted in first order reaches totaling 1.2 Mg C day^{-1} with mean area-normalized fluxes of 25.9 g C m^{-2} day^{-1}. Total fluxes showed a decrease with order until the 3rd order, at which point fluxes increased with order releasing 1.22, 0.58, 0.55, 0.67, and 0.83 Mg C day^{-1} in 1st-5th order stream respectively. The stream network model suggests that GW and benthic hyporheic respiration are the largest sources of CO_2 in river systems accounting for 49.3% and 50.6% of CO_2 emitted respectively, with water column respiration contributing the remaining 0.1% (Figure 5). Absolute GW fluxes show a weak negative correlation with Q ($R = -0.1$) whereas benthic hyporheic and water column respiration showed a strong positive correlation ($R = 0.47$ and 0.52) with Q. In first order streams, GW contributed 84% of the C fluxes, the benthic hyporheic respiration contributed 16%, and the water column contributed 0.04%. In the fourth and fifth order streams benthic hyporheic respiration was 75% and 93% of the fluxes compared to the 25% and 7% contributed by GW and 0.2% from the WC (Figure 6). We note that while precise percent contributions are highly dependent on optimized C_{HZ} values, this overall pattern is a robust feature of the stream network model matching conceptual models of stream CO_2 sources.

The East River and its tributaries feature a number of hotspots of CO_2 emissions, hereafter defined as reaches with fluxes >30 g C m^{-2} day^{-1}. Using this threshold, 10% of the modeled East River watershed by length was identified as a hotspot (Figure 7), with 76% of these hotspots in 1st order streams and 6% in 5th order streams. However, as headwaters are a disproportionate length of the stream, we compared the % hotspots within each order to the total stream length of that order. We found that 1st orders are 15.5% hotspots and that 5th order streams had the second largest proportion of hotspots at 11.4% with 2nd, 3rd, and 4th having 3.4%, 5.2%, and 4.2% respectively. This pattern of hotspots occurring least in mid order streams is consistent with observational data with 1st and 4th order streams having the highest % hotspots by length. Hotspots throughout the modeled and sampled data in the East River watershed had significantly higher slope then the mean of the total network with the modeled watershed having a mean slope of 23% and modeled hotspots having a mean slope of

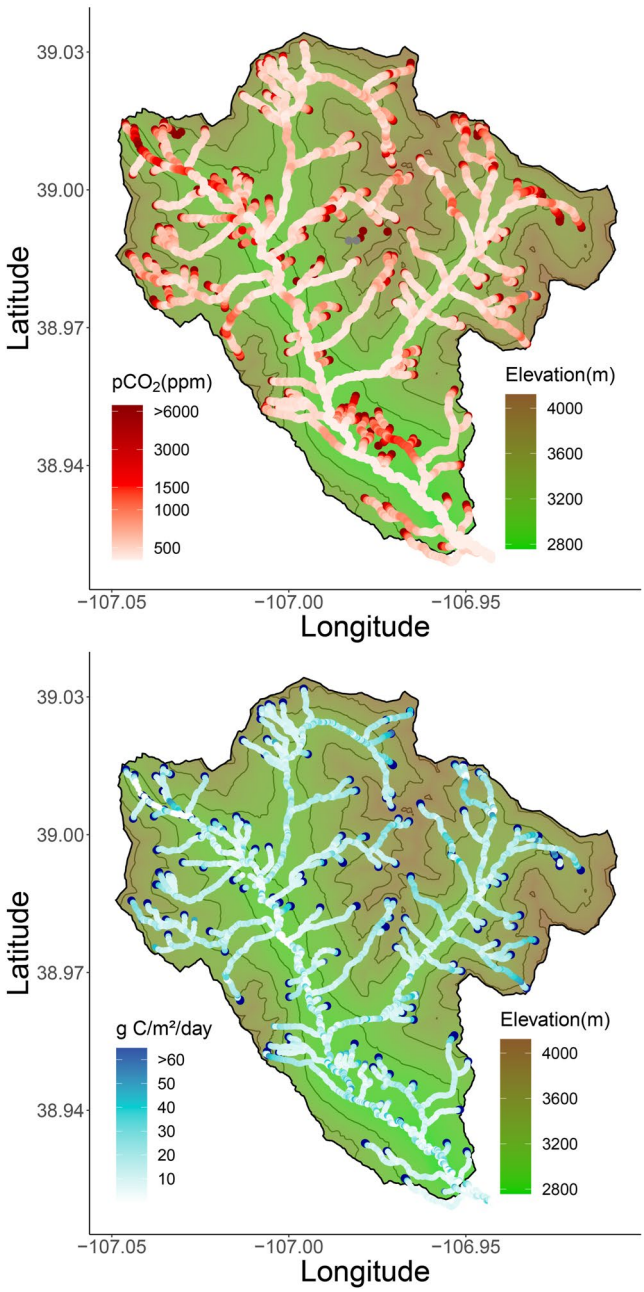


Figure 4. (a) Stream network modeled pCO_2 in the East River shown in red; (b) Stream network model area-normalized CO_2 fluxes shown in blue with fluxes >60 g C/m^2/day shown in black (~1% of stream at locations of stream emergence only).

34% ($p < 10^{-15}$). Comparatively the sampled points had a mean slope of 12% and the sampled hotspots had a mean slope of 21%. The model results show that groundwater dominated hotspots in 1st – 3rd order streams with the BHZ contributing 7%, 22%, and 19% respectively; whereas BHZ respiration was a greater contributor to CO_2 fluxes in 4th and 5th order streams at 78% and 94% respectively (Table S1).

The stream network model outperformed the stepwise MLRM which found Q, velocity, slope, elevation, and mean watershed NPP to be the only significant predictors of pCO_2 (C_{MLRM}), hence referred to as the MLRM. The MLRM

$$C_{MLRM} = 3,600.698 * Q - 8,736.803 * v - 1,227.847 * s - 3.414 * e - 4.182 * NPP + 14,822.450, \quad (17)$$

predicted ln(pCO_2) with a R^2 of 0.21 ($p < 10^{-7}$) and a RMSE of 519 (Figure 3). The RMSE of the MLRM is better than the stream network model as the MLRM preferentially fits the higher pCO_2 values; however, the low R^2 shows that it is worse at predicting pCO_2 variability, particularly below ~1,500 ppm, to the point that negative values are predicted within 2.8% of the East River watershed. Alternatively, the higher RMSE of the stream network model is due to the difficulty in fitting the higher pCO_2 values which is likely due to sensitivity of stream emergence location and spring advection velocities. Additionally, the MLRM predicted a smaller range of pCO_2 (−674 to 3,795 ppm) than the observed data and stream network model that included unrealistic negative values. Using the MLRM across the East River watershed resulted in an estimated CO_2 flux of 47.9 Mg C day^{-1} (50.2 Mg C day^{-1} when excluding negatives) with a mean area normalized flux of 103.8 g C m^{-2} day^{-1} (Table 2).

The MLRM used in Horgby, Segatto, et al. (2019), hence referred to as the Horgby MLRM, was compared to observations and showed less accuracy when predicting ln(pCO_2) with an R^2 of 0.28 $p < 10^{-12}$ RMSE of 1097 (Figure 3), below the $R^2 = 0.39$ $p < 0.001$ in the original paper comparing the MLRM to the data used to generate the model. Importantly, the Horgby MLRM predicts sub-atmospheric pCO_2 values across the watershed in direct contrast with observations. When used to calculate fluxes, this method therefore predicts the East River watershed to be a CO_2 sink, sequestering −16.1 Mg C day^{-1} (Table 2) with an area-normalized mean of −48.5 g C m^{-2} day^{-1}, which is within the 0–−74 g C m^{-2} day^{-1} predicted to be sequestered in the region in the original paper.

4. Discussion

4.1. Stream Network Models Versus Statistical Predictions of pCO_2

To the best of our knowledge this paper represents the first stream network model to predict pCO_2, although the methodology is similar to previous nitrogen stream network models (Gomez-Velez et al., 2015; Gomez-Velez & Harvey, 2014). Here we show that using a high-resolution 10 m DEM and estimated groundwater pCO_2, we are able to predict stream pCO_2 at sub-100 m (22 m mean distance between points) resolution across NHDplus flowlines within the East River watershed. Notably, the model is able to capture structural characteristics of stream CO_2 observations that emerge naturally from the representation of physical processes. These include (a) GW CO_2 hotspots based on spring emergence and topographic convergence, in which stream CO_2 decays over spatial scales of ~10^1–10^2 m depending on the balance of advection and gas exchange (Figure 4); (b) diminish-

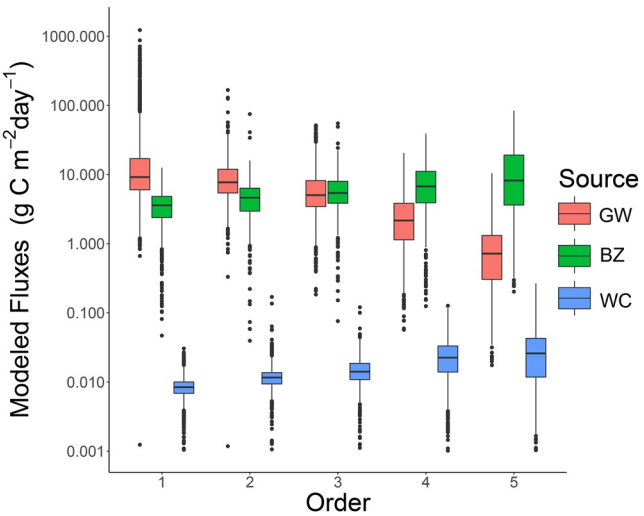


Figure 5. Area-normalized model fluxes grouped by stream order with red (left) box representing groundwater contributions, green (middle) representing BHZ respiration contributions, and blue (right) representing water column contributions of CO_2. One hundred and forty three points not shown for visual clarity that were <0.001 g C m^{-2} day^{-1}.

ing influence of GW inputs with increasing stream size (Figure 6); (c) atmosphere-super-saturated CO_2 in higher-order streams from stream corridor CO_2 production (Figures 4 and 6); and (d) inverse relationships between gas exchange velocities and pCO_2 (Figure 2).

This ability to capture the qualitative structure of spatial variability is borne out by significantly stronger model-data correlations for the stream network model ($R^2 = 0.70$) versus the MLRM ($R^2 = 0.21$) and Horgby MLRM ($R^2 = 0.28$). This structural advantage is even more pronounced when comparing model-data correlation within Strahler stream order. The stream network model predicted ln(pCO_2) with an R^2 of greater than 0.3 across all orders comparatively the MLRM's R^2 was only higher than 0.3 in first order streams (Table 2). This shows that the stream network model has an improved ability to predict pCO_2 within the East River watershed especially within higher order streams as it has improved resolution at lower concentrations. While the MLRM features better RMSE values compared to the stream network model, this is due to the bias of linear regression models to capture extreme values associated with spring emergence as demonstrated by the high model-data R^2 value for 1st order streams. Additionally, the MLRM did not correlate with data from 2nd and 3rd order stream further showing its inability to accurately predict CO_2 at lower concentrations, to the point that negative values are predicted across 2.8% of the East River watershed.

One of the primary reasons MLRM's are unable to capture the structure of stream CO_2 variability across and within stream orders is the implicit treatment of each stream location pCO_2 as independent. In reality, pCO_2 at any given location within the stream network represents a combination of local processes and upstream history. Additionally, as pCO_2 is highly variable at low k_{600} values, the mechanistic connection whereby pCO_2 is limited at high k_{600} (Figure 2a; Rocher-Ros et al., 2019) does not result in a statistical correlation between pCO_2 and k_{600}. These two factors may account for the MLRM points in Figure 2a that have both high pCO_2 (>2,000 ppm) and k_{600} (>~0.1 m/s), leading to an overestimation of C fluxes. Crucially, the inability of MLRM's to capture realistic patterns outside of training datasets (negative pCO_2 values from the MLRM and sub-atmospheric pCO_2 from the Horgby MLRM) suggests that empirical relationships between landscape variables and local pCO_2 involve a large degree of non-stationarity, limiting their transferability or scaling potential. This can be seen in the MLRM as negative values were most common in 1st – 3rd order streams with 29%, 20%, and 48%, of negative predictions respectively, and all negative values were predicted above an elevation of 2,958 m. The Horgby MLRM is strongly dependent on elevation, with sub-atmospheric values predicted above ~3,000 m in the original paper (Horgby, Segatto, et al., 2019). We suggest that this may relate to vegetation in the European Alps versus the Colorado Rockies, in which a lack of high elevation organic matter may limit allochthonous CO_2 sources in the Alps. The limited applicability of MLRM's outside their development region highlights the need for process-based models such as the stream network model presented here, and future work will assess its scalability to other regions.

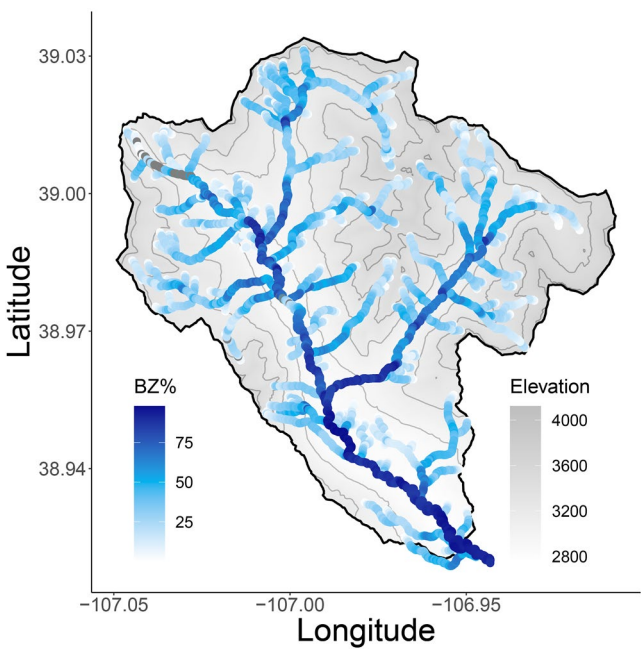


Figure 6. Modeled % benthic hyporheic zone (BHZ) respiration CO_2 contributions at each stream location.

An alternative to MLRM-style analyses was presented in a recent paper which used a machine learning random forest model to predict CO_2 concentrations and fluxes (Martinsen et al., 2020). By using machine learning many of the shortcomings of MLRM's were overcomed. The random forest model was applied to a regional scale across the countries of Denmark, Sweden, and Finland. By using remotely sensed data and calculated CO_2 from 2,298 sites, the model predicted pCO_2 with an R^2 of 0.66 and RMSE of 0.22 $\log_{10}$ [ppm]

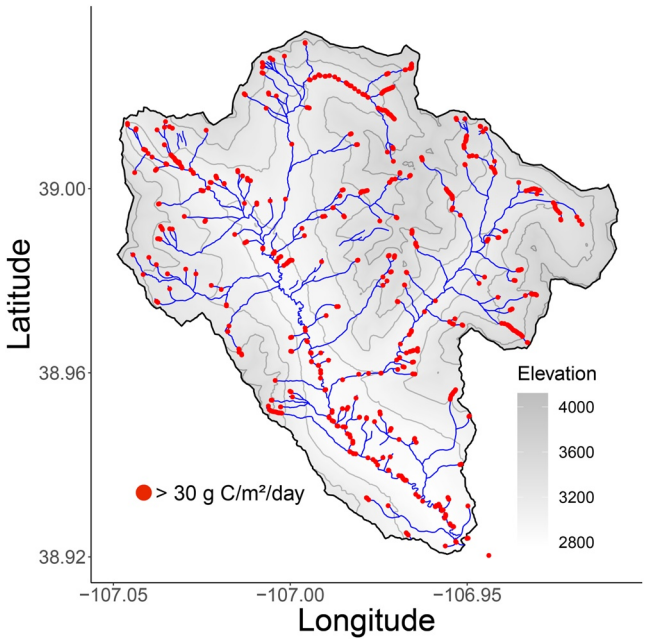


Figure 7. Map of modeled CO_2 flux hotspots. Stream points with area-normalized fluxes greater than 30 g C m^{-2} day^{-1} are shown in colored points with streamlines shown in blue.

which is comparable to the stream network model presented here. However, the random forest model has reduced reliability outside of the training region and excludes 1st and 2nd order streams which are critical hotspots of CO_2 fluxes in rivers. Additionally, process-based models may provide mechanistic insights as to the causes of observable patterns.

As the stream network model represents physical processes, it has the potential to be highly transferable across sites, which will be tested in future research. Notably, data requirements for the stream network model are roughly equivalent to MLRM's and existing estimation methods of gas transfer velocities (e.g., Raymond et al., 2012; Ulseth et al., 2019). In this application, we used stream data observations to optimize free parameters including GW, wetland, water column respiration, and BHZ pCO_2; however, the model may be supplemented in future studies with site-specific measurements of these quantities or empirical models to estimate how these parameters vary across environments. For the proposed stream network model, we did not include spatial variability of optimized free parameters as there is little information to constrain spatial GW pCO_2 and the elevation of the benthic hyporheic zone pCO_2 within the watershed. Additionally, as future work will look to validate this model in different regions and at larger spatial scales, keeping data requirements low was an important goal of the model. Overall, we argue that the stream network model framework represents a significant improvement over existing empirical methods for estimating stream pCO_2.

4.2. Implications for Global Stream CO_2 Fluxes

The improved resolution and pCO_2 estimation of the stream network model allow for a more robust estimation of CO_2 fluxes from the East River. Upscaling methods predicted CO_2 fluxes to be ~4x larger than the stream network model within the East River watershed. The elevated predictions from statistical upscaling methods likely stem from an overestimation of pCO_2 in reaches with high k_{CO2} as the estimated CO_2 concentrations are likely higher than would be expected at these locations (Figure 2). Observations were also biased towards relatively flat areas with higher pCO_2, as many steep reaches within sampled streams were inaccessible. Additionally, the structure of pCO_2 data lends itself to further overestimation as it commonly is right-skewed with few large CO_2 concentrations causing the mean to be larger than the median and mode (Figure S8 and Text S4 in Supporting Information S1). As described above, the Horgby MLRM estimates the East River as a CO_2 sink, which suggests their estimates of global mountainous stream CO_2 fluxes may be artificially low. The MLRM predicted a CO_2 flux 12x greater than the stream network model even though 14% of the model was predicted to be a CO_2 sink; this is likely due to the prediction of pCO_2 values above 2,000 ppm at relatively high k_{600} > 0.06 m/s (Figure 2) as hypothesized by Rocher-Ros et al. (2019). The overestimation of CO_2 fluxes seen here confirm that spatial mismatches between model variables represent an important issue in current stream CO_2 emission estimates.

Taken together, these analyses support the idea that current global budgets may overestimate CO_2 fluxes from rivers and streams as suggested by Rocher-Ros et al. (2019). While site-based discrepancies between upscaling and MLRM versus stream network fluxes are high (400%–1,200%), we note that these discrepancies are likely maximized due to the mountainous terrain and elevated gas exchange velocities. Future work will target how these methods compare across different hydrologic conditions (e.g., peak snowmelt vs. baseflow), along with the impact of k-pCO_2 inverse relationships in lowland environments and at regional to global scales. Notably, this may result in a downward revision in global stream CO_2 estimates, as has recently been suggested (Rocher-Ros et al., 2019).

4.3. Internal Production Versus External Inputs

The proportion of external and internal sources of CO_2 fluxes in streams is an active area of research, as relative contributions from GW, the soil zone, water column respiration, photodegradation, and the hyporheic zone remain uncertain (Cory et al., 2014; Lupon et al., 2019; Winterdahl et al., 2016). Quantifying internal and external sources of CO_2 is difficult and requires extensive field experiments to create C budgets for individual reaches (e.g., Hotchkiss et al., 2015; Lupon et al., 2019; Rasilo et al., 2017). This has limited our broader understanding of CO_2 sources as these field and data intensive studies do not sufficiently cover the range of stream orders, discharges, or landscape characteristics that control the processes contributing to stream CO_2. However, using the full stream network model, we are able to estimate the proportions of CO_2 from internal and external sources that are consistent with field observations from the East River watershed and larger-scale data compilations.

As described above, the model predicts diminishing influence of GW inputs with increasing stream size, consistent with previous studies (Hotchkiss et al., 2015). Additionally, the stream network model suggests that water-column respiration is the smallest contributor of the modeled processes to stream network CO_2 fluxes within the studied watershed. This result is clear using optimized WC respiration and is also robust across sensitivity analyses featuring a 38x increase in WC respiration rates (Figure S5 in Supporting Information S1). This result is also consistent with the budget analysis of Rasilo et al. (2017) for 1st-3rd order streams in the Cote du Nord region. We note that water-column respiration likely becomes increasingly important at larger stream sizes (Reisinger et al., 2021) as has been noted for N_2O production (Marzadri et al., 2017).

The stream network model further suggests that respiration within the benthic hyporheic zone is the primary source of CO_2 in 4th and 5th order streams, consistent with Rasilo et al. (2017) and contrasting with Hotchkiss et al. (2015). This inconsistency in previous studies likely stems from methodological differences, as whole stream metabolism can incorporate uncertainty from reaeration and GW O_2, whereas net changes in DOC reflect the processes of GPP, ER, terrestrial export, and production of DOC within the hyporheic zone (Rasilo et al., 2017; Rocher-Ros et al., 2020). We note that the model-data statistical agreement is relatively insensitive to the precise value of BHZ pCO_2 used, which itself is likely highly variable across the East River; however, our optimized value agrees well with estimates based on previously published BHZ pore water geochemistry from the main stem of the East River (Nelson et al., 2019; Text S2 in Supporting Information S1).

Assuming BHZ CO_2 fluxes are supported solely via the oxidation of stream DOC, the modeled BHZ fluxes would require the input of 1,867 mol C km^{-2} day^{-1} of DOC from the terrestrial landscape to support these respiration rates. This value is significantly higher than measured stream DOC fluxes at the time of sampling which ranged from 12 to 416 mol C km^{-2} day^{-1}, though we note that in-stream measurements reflected processed concentrations rather than direct terrestrial exports. Further, modeled DOC requirements fall within range of seasonal DOC exports within the East River watershed (>2,600 mol C km^{-2} day^{-1}; Winnick et al., 2017) and are consistent with DOC export requirements in the synthesis of Mineau et al. (2016). In addition to stream water-derived DOC, BHZ respiration is also supported by the production of DOC from buried organic matter, which in some cases may account for >75% of BHZ CO_2 production (Findlay et al., 1993). Particulate organic carbon (POC) was not measured within our study. However, the deposition of particulate organic matter can supply carbon at rates of ~0.02–0.4 mol C m^{-2} day^{-1} (Richardson et al., 2009). POC can store up to 558 mol C m^{-2} within the streambed (Metzler & Smock, 1990). If these findings are applicable to the East River system, they would reconcile the measured DOC fluxes and model requirements. Additionally, the mean in-stream fluxes (0.48 mol C m^{-2} day^{-1}) (Figure 5) fall within reported ecosystem respiration rates for similar sized watersheds (0.02–0.63 mol C m^{-2} day^{-1}) (Hoellein et al., 2013). Despite its potential role in controlling higher-order stream CO_2 concentrations and fluxes, very few studies have sought to characterize the dynamics of BHZ carbon production, which instead have focused primarily on nitrogen and oxygen dynamics. Thus, an improved understanding of BHZ CO_2 production and exchange is strongly needed to accurately estimate stream CO_2 concentrations and fluxes.

Although overarching patterns of decreasing external contributions with order hold across the range of modeled BHZ pCO_2, a mosaic of BHZ and GW dominated sections exist within mid order stream showing that small scale variability plays an important role (Boodoo et al., 2019; Krause et al., 2017). This can be seen most readily within 3rd order streams where 49% of the stream length is GW-dominated (Figures 5 and 6). In 2nd and 4th order streams we see less extreme patchiness with 80% and 6% of streams by length GW dominated respectively. This

emphasizes that local conditions may deviate from predicted patterns, as these transitions within stream systems represent a patchwork dynamic rather than a smooth gradient (Boodoo et al., 2019; Krause et al., 2017).

4.4. Hotspots

The magnitude and spatial distribution of carbon fluxes has been the focus of many studies, which have found headwaters to be hotspots of CO_2 fluxes, defined here as locations with CO_2 fluxes greater than 30 g C m^{-2} day^{-1}. More recent studies have begun to characterize the interplay of topographically driven evasion and sources of CO_2 which create a mosaic of fluxes and hotspots through stream systems (Duvert et al., 2018; Rocher-Ros et al., 2019). In the past, upscaling and coarse resolution MLRM's have hindered our ability to parse out where in landscapes these hotspots are. Using the stream network model, we predict where in the landscape these hotspots are and their relative contribution to integrated fluxes across stream orders. From this we suggest that first order streams are the largest contributors, making up 76% of watershed hotspots (Figure 7), consistent with findings from Duvert et al. (2018). However, 5th order streams feature higher proportional hotspot areas as compared to 2nd–4th order streams in the East River, showing that mid-order streams have the potential to be an important source of CO_2 fluxes. Although 5th order streams may have more hotspots then previously surmised, they are still of a smaller magnitude than 1st order streams as the total fluxes were still greater in 1st order streams.

Hotspots in the East River and its tributaries were more likely to feature GW as the primary source of CO_2, with 90% of hotspots by length receiving greater than 50% of their CO_2 from GW. Comparatively, only 71% of the East River and its tributaries by length had GW as a primary source of CO_2. This pattern of GW-supplied hotspots held in 1st–2nd order streams but inverted in 4th and 5th order streams where hotspots had the majority of their CO_2 supplied by BHZ respiration. The location of this transition has additional significance as 3rd–4th order streams are where the switch from GW to BHZ dominated inputs occurs, showing that hotspots are not purely groundwater supplied but instead can be supplied through internally produced pCO_2. Additionally, the mean slope of hotspots is steeper than the mean stream slope of the East River and its tributaries showing that hotspots likely occur in areas that transition from low to high slopes, in which CO_2 that has built up in low slope reaches is quickly lost when k increases, similar to previous findings (Rocher-Ros et al., 2019). As stream network models are able to predict hotspots and parse out CO_2 sources and topographic controls in actual stream environments, they may further provide the ability to guide targeted field sampling.

5. Conclusions

Predicting regional and global stream CO_2 emissions remains challenging, and estimates continue to change due to additional sources of data and methodological improvements (Drake et al., 2018). Many of these improvements include additional sources of error including mismatches between data resolution which can become significant when upscaling as suggested by Rocher-Ros et al. (2019). Here, we tested the ability of a stream network model to improve predictions of stream CO_2 concentrations through representation of physical hydrologic processes, including atmospheric gas exchange, downstream advection, groundwater inputs of CO_2, and benthic hyporheic respiration driven by turbulent exchange. These process-based predictions outperform statistical methods within the East River watershed, and future work will test the accuracy of the stream network model when applied across annual hydrologic conditions and to other systems. The stream network model also provides direct estimates of the proportion of external and internal CO_2 contributions, suggesting that benthic hyporheic exchange represents a significant portion of stream CO_2, contributing 51% across the watershed at the time of sampling. Finally, through the direct comparison of existing statistical methods to the stream network model and sample data, we found that statistical upscaling of pCO_2 can result in a significant overestimation of CO_2 fluxes within the East River watershed. Future work is therefore needed to quantify potential overestimation of regional and global scale stream CO_2 fluxes by statistical methods.

Data Availability Statement

All data and code used in this work are available in Supporting Information S1; further, the data set is available through HydroShare and can be accessed through the link http://www.hydroshare.org/resource/9f907b46baa848e180c49339d605bf31.

Acknowledgments
We thank Jennifer Reithel, Ian Billick, and the Rocky Mountain Biological Laboratory staff for field and logistical support. We also thank Kate Maher, Corey Lawrence, Ken Williams, Rosemary Carroll, David Boutt, and the Hydroseminar group at UMass Geosciences for useful conversations related to this paper. We thank Gerard Rocher-Ros, David Butman, and two anonymous reviewers whose comments and suggestions improved earlier versions of this manuscript. This work was supported by the National Science Foundation (EAR-2103520) and UMass Faculty Startup Funds to MJ Winnick.

References

Allen, G. H., & Pavelsky, T. M. (2018). Global extent of rivers and streams. *Science*, *361*(6402), 585–588. https://doi.org/10.1126/science.aat0636

Battaglin, W., Hay, L., & Markstrom, S. (2011). Simulating the potential effects of climate change in two Colorado basins and at two Colorado ski areas. *Earth Interactions*, *15*, 1–23. https://doi.org/10.1175/2011EI373.1

Bencala, K. E., & Walters, R. A. (1983). Simulation of solute transport in a mountain pool-and-riffle stream: A transient storage model. *Water Resources Research*, *19*(3), 718–724. https://doi.org/10.1029/WR019i003p00718

Bernhardt, E. S., Heffernan, J. B., Grimm, N. B., Stanley, E. H., Harvey, J. W., Arroita, M., et al. (2018). The metabolic regimes of flowing waters. *Limnology & Oceanography*, *63*, S99–S118. https://doi.org/10.1002/lno.10726

Boodoo, K. S., Schelker, J., Trauth, N., Battin, T. J., & Schmidt, C. (2019). Sources and variability of CO_2 in a prealpine stream gravel bar. *Hydrological Processes*, *33*(17), 2279–2299. https://doi.org/10.1002/hyp.13450

Borges, A. V., Darchambeau, F., Teodoru, C. R., Marwick, T. R., Tamooh, F., Geeraert, N., et al. (2015). Globally significant greenhouse-gas emissions from African inland waters. *Nature Geoscience*, *8*(8), 637–642. https://doi.org/10.1038/ngeo2486

Breugem, W., Boersma, B., & Uittenbogaard, R. (2006). The influence of wall permeability on turbulent channel flow. *Journal of Fluid Mechanics*, *562*, 35–72. https://doi.org/10.1017/S0022112006000887

Buffam, I., Laudon, H., Bishop, K., Öquist, M., & Wallin, M. (2010). Temporal and spatial variability of dissolved inorganic carbon in a boreal stream network: Concentrations and downstream fluxes. *Journal of Geophysical Research*, *115*(G2), G02014. https://doi.org/10.1029/2009jg001100

Butman, D., & Raymond, P. A. (2011). Significant efflux of carbon dioxide from streams and rivers in the United States. *Nature Geoscience*, *4*, 839–842. https://doi.org/10.1038/ngeo1294

Carroll, R., Newman, A., Beutler, C., & Williams, K. (2021). *Stream discharge data collected within the East River, Colorado for the Lawrence Berkeley National Laboratory watershed function science focus area (water years 2019 to 2020)*. https://doi.org/10.15485/1779721

Carroll, R., & Williams, K. (2019). *Discharge data collected within the East River for the Lawrence Berkeley National Laboratory watershed function science focus area (water years 2015-present)*. https://doi.org/10.21952/WTR/1495380

Carroll, R. W. H., Bearup, L. A., Brown, W., Dong, W., Bill, M., & Willlams, K. H. (2018). Factors controlling seasonal groundwater and solute flux from snow-dominated basins. *Hydrological Processes*, *32*(14), 2187–2202. https://doi.org/10.1002/hyp.13151

Cole, J. J., Prairie, Y. T., Caraco, N. F., McDowell, W. H., Tranvik, L. J., Striegl, R. G., et al. (2007). Plumbing the global carbon cycle: Integrating inland waters into the terrestrial carbon budget. *Ecosystems*, *10*, 171–185. https://doi.org/10.1007/s10021-006-9013-8

Cory, R. M., Ward, C. P., Crump, B. C., & Kling, G. W. (2014). Sunlight controls water column processing of carbon in arctic fresh waters. *Science*, *345*(6199), 925–928. https://doi.org/10.1126/science.1253119

Drake, T. W., Raymond, P. A., & Spencer, R. G. M. (2018). Terrestrial carbon inputs to inland waters: A current synthesis of estimates and uncertainty. *Limnology and Oceanography Letters*, *3*(3), 132–142. https://doi.org/10.1002/lol2.10055

Duvert, C., Butman, D. E., Marx, A., Ribolzi, O., & Hutley, L. B. (2018). CO_2 evasion along streams driven by groundwater inputs and geomorphic controls. *Nature Geoscience*, *11*(11), 813–818. https://doi.org/10.1038/s41561-018-0245-y

Elberling, B., Askaer, L., Jørgensen, C. J., Joensen, H. P., Kühl, M., Glud, R. N., & Lauritsen, F. R. (2011). Linking Soil O_2, CO_2, and CH_4 concentrations in a wetland soil: Implications for CO_2 and CH_4 fluxes. *Environmental Science & Technology*, *45*, 3393–3399. https://doi.org/10.1021/es103540k

Findlay, S., Strayer, D., Goumbala, C., & Gould, K. (1993). Metabolism of streamwater dissolved organic carbon in the shallow hyporheic zone. *Limnology & Oceanography*, *38*(7), 1493–1499. https://doi.org/10.4319/LO.1993.38.7.1493

Gaskill, D. L., Godwin, L. H., & Mutschler, F. E. (1967). *Geologic map of the Oh-Be-Joyful quadrangle, Gunnison County, Colorado*. Geologic Quadrangle. https://doi.org/10.3133/gq578

Gaskill, D. L., Mutschler, F. E., Kramer, J. H., Thomas, J. A., & Zahony, S. G. (1991). *Geologic map of the Gothic quadrangle, Gunnison County, Colorado*.

Gomez-Velez, J. D., & Harvey, J. W. (2014). A hydrogeomorphic river network model predicts where and why hyporheic exchange is important in large basins. *Geophysical Research Letters*, *41*(18), 6403–6412. https://doi.org/10.1002/2014GL061099

Gomez-Velez, J. D., Harvey, J. W., Cardenas, M. B., & Kiel, B. (2015). Denitrification in the Mississippi River network controlled by flow through river bedforms. *Nature Geoscience*, *8*(12), 941–945. https://doi.org/10.1038/ngeo2567

Grant, S. B., Azizian, M., Cook, P., Boano, F., & Rippy, M. A. (2018). Factoring stream turbulence into global assessments of nitrogen pollution. *Science*, *359*(6381), 1266–1269. https://doi.org/10.1126/science.aap8074

Grant, S. B., Gomez-Velez, J. D., & Ghisalberti, M. (2018). Modeling the effects of turbulence on hyporheic exchange and local-to-global nutrient processing in streams. *Water Resources Research*, *54*(9), 5883–5889. https://doi.org/10.1029/2018WR023078

Harvey, J., Gomez-Velez, J., Schmadel, N., Scott, D., Boyer, E., Alexander, R., et al. (2019). How hydrologic connectivity regulates water quality in river corridors. *JAWRA Journal of the American Water Resources Association*, *55*(2), 369–381. https://doi.org/10.1111/1752-1688.12691

Harvey, J. W., Böhlke, J. K., Voytek, M. A., Scott, D., & Tobias, C. R. (2013). Hyporheic zone denitrification: Controls on effective reaction depth and contribution to whole-stream mass balance. *Water Resources Research*, *49*(10), 6298–6316. https://doi.org/10.1002/wrcr.20492

Hengl, T., De Jesus, J. M., Heuvelink, G. B. M., Gonzalez, M. R., Kilibarda, M., Blagotić, A., et al. (2017). SoilGrids250m: Global gridded soil information based on machine learning. *PLoS One*, *12*(2), e0169748. https://doi.org/10.1371/journal.pone.0169748

Hilton, R. G., Turowski, J. M., Winnick, M., Dellinger, M., Schleppi, P., Williams, K. H., et al. (2021). Concentration-discharge relationships of dissolved rhenium in Alpine catchments reveal its use as a tracer of oxidative weathering. *Water Resources Research*, *57*, e2021WR029844. https://doi.org/10.1029/2021WR029844

Hoellein, T. J., Bruesewitz, D. A., & Richardson, D. C. (2013). Revisiting Odum (1956): A synthesis of aquatic ecosystem metabolism. *Limnology & Oceanography*, *58*(6), 2089–2100. https://doi.org/10.4319/lo.2013.58.6.2089

Hope, D., Palmer, S. M., Billett, M. F., & Dawson, J. J. C. (2004). Variations in dissolved CO_2 and CH_4 in a first-order stream and catchment: An investigation of soil-stream linkages. *Hydrological Processes*, *18*(17), 3255–3275. https://doi.org/10.1002/hyp.5657

Horgby, Å., Boix Canadell, M., Ulseth, A. J., Vennemann, T. W., & Battin, T. J. (2019). High-resolution spatial sampling identifies groundwater as driver of CO_2 dynamics in an Alpine stream network. *Journal of Geophysical Research: Biogeosciences*, *124*(7), 1961–1976. https://doi.org/10.1029/2019JG005047

Horgby, Å., Segatto, P. L., Bertuzzo, E., Lauerwald, R., Lehner, B., Ulseth, A. J., et al. (2019). Unexpected large evasion fluxes of carbon dioxide from turbulent streams draining the world's mountains. *Nature Communications*, *10*(1), 4888. https://doi.org/10.1038/s41467-019-12905-z

Horn, B. K. P. (1981). Hill shading and the reflectance map. *Proceedings of the IEEE*, *69*(1), 14–47. https://doi.org/10.1109/PROC.1981.11918

Hotchkiss, E. R., Hall, R. O., Jr, Sponseller, R. A., Butman, D., Klaminder, J., Laudon, H., et al. (2015). Sources of and processes controlling CO_2 emissions change with the size of streams and rivers. *Nature Geoscience*, *8*(9), 696–699. https://doi.org/10.1038/ngeo2507

Hubbard, S. S., Williams, K. H., Agarwal, D., Banfield, J., Beller, H., Bouskill, N., et al. (2018). The East River, Colorado, Watershed: A mountainous community testbed for improving predictive understanding of multiscale hydrological-biogeochemical dynamics. *Vadose Zone Journal*, *17*(1), 1–25, 180061. https://doi.org/10.2136/vzj2018.03.0061

Hunt, C. W., Snyder, L., Salisbury, J. E., Vandemark, D., & McDowell, W. H. (2017). SIPCO2: A simple, inexpensive surface water pCO_2 sensor. *Limnology and Oceanography: Methods*, *15*, 291–301. https://doi.org/10.1002/lom3.10157

Jähne, B., Heinz, G., & Dietrich, W. (1987). Measurement of the diffusion coefficients of sparingly soluble gases in water. *Journal of Geophysical Research*, *92*(C10), 10767. https://doi.org/10.1029/JC092iC10p10767

Johnson, M. S., Billett, M. F., Dinsmore, K. J., Wallin, M., Dyson, K. E., & Jassal, R. S. (2010). Direct and continuous measurement of dissolved carbon dioxide in freshwater aquatic systems-method and applications. *Ecohydrology*, *3*, 68–78. https://doi.org/10.1002/eco.95

Johnson, M. S., Lehmann, J., Riha, S. J., Krusche, A. V., Richey, J. E., Ometto, J. P. H. B., & Couto, E. G. (2008). CO_2 efflux from Amazonian headwater streams represents a significant fate for deep soil respiration. *Geophysical Research Letters*, *35*(17), 1–5. https://doi.org/10.1029/2008GL034619

Koschorreck, M., Prairie, Y. T., Kim, J., & Marcé, R. (2021). Technical note: CO_2 is not like CH_4- Limits of and corrections to the headspace method to analyse pCO_2 in fresh water. *Biogeosciences*, *18*, 1619–1627. https://doi.org/10.5194/bg-18-1619-2021

Krause, S., Lewandowski, J., Grimm, N. B., Hannah, D. M., Pinay, G., McDonald, K., et al. (2017). Ecohydrological interfaces as hot spots of ecosystem processes. *Water Resources Research*, *53*, 6359–6376. https://doi.org/10.1002/2016WR019516

Lauerwald, R., Laruelle, G. G., Hartmann, J., Ciais, P., & Regnier, P. A. G. (2015). Spatial patterns in CO_2 evasion from the global river network. *Global Biogeochemical Cycles*, *29*(5), 534–554. https://doi.org/10.1002/2014GB004941

Li, A., Aubeneau, A. F., Bolster, D., Tank, J. L., & Packman, A. I. (2017). Covariation in patterns of turbulence-driven hyporheic flow and denitrification enhances reach-scale nitrogen removal. *Water Resources Research*, *53*(8), 6927–6944. https://doi.org/10.1002/2016WR019949

Lupon, A., Denfeld, B. A., Laudon, H., Leach, J., Karlsson, J., & Sponseller, R. A. (2019). Groundwater inflows control patterns and sources of greenhouse gas emissions from streams. *Limnology & Oceanography*, *64*(4), 1545–1557. https://doi.org/10.1002/lno.11134

Markstrom, S. L., & Hay, L. E. (2009). Integrated watershed scale response to climate change for selected basins across the United States. *American Water Resources Association*, *11*(2), 8–10.

Martinsen, K. T., Kragh, T., & Sand-Jensen, K. (2020). Carbon dioxide partial pressure and emission throughout the scandinavian stream network. *Global Biogeochemical Cycles*, *34*(12), e2020GB006703. https://doi.org/10.1029/2020GB006703

Marx, A., Dusek, J., Jankovec, J., Sanda, M., Vogel, T., van Geldern, R., et al. (2017). A review of CO_2 and associated carbon dynamics in headwater streams: A global perspective. *Reviews of Geophysics*, *55*(2), 560–585. https://doi.org/10.1002/2016RG000547

Marzadri, A., Dee, M. M., Tonina, D., Bellin, A., & Tank, J. L. (2017). Role of surface and subsurface processes in scaling N_2O emissions along riverine networks. *Proceedings of the National Academy of Sciences of the United States of America*, *114*(17), 4330–4335. https://doi.org/10.1073/pnas.1617454114

Metzler, G. M., & Smock, L. A. (1990). Storage and dynamics of subsurface detritus in a sand-bottomed stream. *Canadian Journal of Fisheries and Aquatic Sciences*, *47*(3), 588–594. https://doi.org/10.1139/f90-067

Mineau, M. M., Wollheim, W. M., Buffam, I., Findlay, S. E. G., Hall, R. O., Hotchkiss, E. R., et al. (2016). Dissolved organic carbon uptake in streams: A review and assessment of reach-scale measurements. *Journal of Geophysical Research: Biogeosciences*, *121*(8), 2019–2029. https://doi.org/10.1002/2015JG003204

Morrison, S. J., Goodknight, C. S., Tigar, A. D., Bush, R. P., & Gil, A. (2012). Naturally occurring contamination in the Mancos Shale. *Environmental Science & Technology*, *46*, 1379–1387. https://doi.org/10.1021/es203211z

NASA. (2019). *MODIS gross primary production (GPP)/Net primary production (NPP)*. Retrieved from https://modis.gsfc.nasa.gov/data/dataprod/mod17.php

Nelson, A. R., Sawyer, A. H., Gabor, R. S., Saup, C. M., Bryant, S. R., Harris, K. D., et al. (2019). Heterogeneity in hyporheic flow, pore water chemistry, and microbial community composition in an Alpine streambed. *Journal of Geophysical Research: Biogeosciences*, *124*(11), 3465–3478. https://doi.org/10.1029/2019JG005226

Newcomer, M., & Rogers, D. B. (2020). *Gap-filled meteorological data (2011-2020) and modeled potential evapotranspiration data from the KCOMTCRE2 WeatherUnderground weather station, from the East River Watershed, Colorado*. Watershed Function SFA. https://doi.org/10.15485/1734790

O'Connor, B. L., & Hondzo, M. (2008). Dissolved oxygen transfer to sediments by sweep and eject motions in aquatic environments. *Limnology & Oceanography*, *53*(2), 566–578. https://doi.org/10.4319/lo.2008.53.2.0566

Packman, A. I., Salehin, M., & Zaramella, M. (2004). Hyporheic exchange with gravel beds: Basic hydrodynamic interactions and bedform-induced advective flows. *Journal of Hydraulic Engineering*, *130*(7), 647–656. https://doi.org/10.1061/(asce)0733-9429(2004)130:7(647)

Plummer, L. N., & Busenberg, E. (1982). The solubilities of calcite, aragonite and vaterite in CO_2-H_2O solutions between 0 and 90°C, and an evaluation of the aqueous model for the system $CaCO_3$-CO_2-H_2O. *Geochimica et Cosmochimica Acta*, *46*(6), 1011–1040. https://doi.org/10.1016/0016-7037(82)90056-4

PRISM. (2013). *Parameter-elevation regressions on independent slopes model*. Retrieved from http://www.prism.oregonstate.edu/normals/

R Core Team. (2020). R: *A language and environment for statistical computing*. R Foundation for Statistical Computing. Retrieved from https://www.r-project.org

Rasilo, T., Hutchins, R. H. S., Ruiz-González, C., & del Giorgio, P. A. (2017). Transport and transformation of soil-derived CO_2, CH_4 and DOC sustain CO_2 supersaturation in small boreal streams. *The Science of the Total Environment*, *579*, 902–912. https://doi.org/10.1016/j.scitotenv.2016.10.187

Raymond, P. A., Hartmann, J., Lauerwald, R., Sobek, S., Mcdonald, C., Hoover, M., et al. (2013). Global carbon dioxide emissions from inland waters. *Nature*, *503*(7476), 355–359. https://doi.org/10.1038/nature12760

Raymond, P. A., Zappa, C. J., Butman, D., Bott, T. L., Potter, J., Mulholland, P., et al. (2012). Scaling the gas transfer velocity and hydraulic geometry in streams and small rivers. *Limnology and Oceanography: Fluids and Environments*, *2*(1), 41–53. https://doi.org/10.1215/21573689-1597669

Reisinger, A. J., Tank, J. L., Hall, R. O., Rosi, E. J., Baker, M. A., & Genzoli, L. (2021). Water column contributions to the metabolism and nutrient dynamics of mid-sized rivers. *Biogeochemistry*, *153*(1), 67–84. https://doi.org/10.1007/s10533-021-00768-w

Reisinger, A. J., Tank, J. L., Rosi-Marshall, E. J., Hall, R. O., & Baker, M. A. (2015). The varying role of water column nutrient uptake along river continua in contrasting landscapes. *Biogeochemistry*, *125*(1), 115–131. https://doi.org/10.1007/s10533-015-0118-z

Richardson, J. S., Hoover, T. M., & Lecerf, A. (2009). Coarse particulate organic matter dynamics in small streams: Towards linking function to physical structure. *Freshwater Biology*, *54*(10), 2116–2126. https://doi.org/10.1111/J.1365-2427.2009.02279.X

Roche, K. R., Shogren, A. J., Aubeneau, A., Tank, J. L., & Bolster, D. (2019). Modeling benthic versus hyporheic nutrient uptake in unshaded streams with varying substrates. *Journal of Geophysical Research: Biogeosciences*, *124*(2), 367–383. https://doi.org/10.1029/2018JG004684

Rocher-Ros, G., Sponseller, R. A., Bergström, A. K., Myrstener, M., & Giesler, R. (2020). Stream metabolism controls diel patterns and evasion of CO_2 in Arctic streams. *Global Change Biology*, *26*(3), 1400–1413. https://doi.org/10.1111/gcb.14895

Rocher-Ros, G., Sponseller, R. A., Lidberg, W., Mörth, C., & Giesler, R. (2019). Landscape process domains drive patterns of CO_2 evasion from river networks. *Limnology and Oceanography Letters*, *4*, 87–95. https://doi.org/10.1002/lol2.10108

Sawakuchi, H. O., Neu, V., Ward, N. D., Barros, M. D. L. C., Valerio, A. M., Gagne-Maynard, W., et al. (2017). Carbon dioxide emissions along the lower Amazon River. *Frontiers in Marine Science*, *4*, 76. https://doi.org/10.3389/fmars.2017.00076

Steefel, C. I., DePaolo, D. J., & Lichtner, P. C. (2005). Reactive transport modeling: An essential tool and a new research approach for the Earth sciences. *Earth and Planetary Science Letters*, *240*, 539–558. https://doi.org/10.1016/j.epsl.2005.09.017

Stets, E. G., Butman, D., McDonald, C. P., Stackpoole, S. M., DeGrandpre, M. D., & Striegl, R. G. (2017). Carbonate buffering and metabolic controls on carbon dioxide in rivers. *Global Biogeochemical Cycles*, *31*(4), 663–677. https://doi.org/10.1002/2016GB005578

Ulseth, A. J., Hall, R. O., Boix Canadell, M., Madinger, H. L., Niayifar, A., & Battin, T. J. (2019). Distinct air–water gas exchange regimes in low- and high-energy streams. *Nature Geoscience*, *12*(4), 259–263. https://doi.org/10.1038/s41561-019-0324-8

U.S. Geological Survey. (2016). *GAP/LANDFIRE national terrestrial ecosystems 2011*. U.S. Geological Survey Data Release. https://doi.org/10.5066/F7ZS2TM0

U.S. Geological Survey (2019). National hydrography dataset plus high resolution. Retrieved from https://www.usgs.gov/core-science-systems/ngp/national-hydrography/nhdplus-high-resolution

Wanninkhof, R. (1992). Relationship between wind speed and gas exchange over the ocean. *Journal of Geophysical Research*, *97*(C5), 7373–7382. https://doi.org/10.1029/92JC00188

Ward, N. D., Keil, R. G., Medeiros, P. M., Brito, D. C., Cunha, A. C., Dittmar, T., et al. (2013). Degradation of terrestrially derived macromolecules in the Amazon River. *Nature Geoscience*, *6*(7), 530–533. https://doi.org/10.1038/ngeo1817

Winnick, M. J. (2021). Stream transport and substrate controls on nitrous oxide yields from hyporheic zone denitrification. *AGU Advances*, *2*(4), e2021AV000517. https://doi.org/10.1029/2021AV000517

Winnick, M. J., Carroll, R. W. H., Williams, K. H., Maxwell, R. M., Dong, W., & Maher, K. (2017). Snowmelt controls on concentration-discharge relationships and the balance of oxidative and acid-base weathering fluxes in an alpine catchment, East River, Colorado. *Water Resources Research*, *53*(3), 2507–2523. https://doi.org/10.1002/2016WR019724

Winnick, M. J., Lawrence, C. R., McCormick, M., Druhan, J. L., & Maher, K. (2020). Soil respiration response to rainfall modulated by plant phenology in a montane meadow, East River, Colorado, USA. *Journal of Geophysical Research: Biogeosciences*, *125*(10). https://doi.org/10.1029/2020JG005924

Winterdahl, M., Wallin, M. B., Karlsen, R. H., Laudon, H., Öquist, M., & Lyon, S. W. (2016). Decoupling of carbon dioxide and dissolved organic carbon in boreal headwater streams. *Journal of Geophysical Research: Biogeosciences*, *121*(10), 2630–2651. https://doi.org/10.1002/2016JG003420

Reference From the Supporting Information

Steefel, C. I., Appelo, C. A. J., Arora, B., Jacques, D., Kalbacher, T., Kolditz, O., et al. (2015). Reactive transport codes for subsurface environmental simulation. *Computational Geosciences*, *19*(3), 445–478. https://doi.org/10.1007/s10596-014-9443-x